Adaptive smartphone-based sensor fusion for estimating competitive rowing kinematic metrics

Bryn Cloud[1], Britt Tarien[1], Ada Liu[1], Thomas Shedd[1], Xinfan Lin[1], Mont Hubbard[1], Paul Crawford[2], Jason K. Moore[1]*

1 Mechanical and Aerospace Engineering, University of California, Davis, California, USA
2 Hegemony Technologies LLC, Davis, California, USA

* jkm@ucdavis.edu

Abstract

Competitive rowing highly values boat position and velocity data for real-time feedback during training, racing and post-training analysis. The ubiquity of smartphones with embedded position (GPS) and motion (accelerometer) sensors motivates their possible use in these tasks. In this paper, we investigate the use of two real-time digital filters to achieve highly accurate but reasonably priced measures of boat speed and distance traveled. Both filters combine acceleration and location data to estimate boat distance and speed; the first using a complementary frequency response-based filter technique, the second with a Kalman filter formalism that includes adaptive, real-time estimates of effective accelerometer bias. The estimates of distance and speed from both filters were validated and compared with accurate reference data from a 10 Hz differential GPS system with better than 1 cm precision, in experiments using two subjects (an experienced club-level rower and an elite rower) in two different boats on a 300 m course. Relative to single channel (smartphone GPS only) measures of distance and speed, the complementary filter improved the accuracy and precision of boat speed, boat distance traveled, and distance per stroke by 44%, 42%, and 73%, respectively, while the Kalman filter improved the accuracy and precision of boat speed and distance per stroke by 51% and 72%, respectively. Both filters demonstrate promise as general purpose methods to substantially improve estimates of important rowing performance metrics.

Introduction

Non-intrusive collection of data from athletes during practice and competition provides opportunities for evidenced-based performance evaluation and coaching. Traditional kinematic measurement techniques in sports have frequently required elaborate equipment to capture the motion of human body segments and associated sports equipment; see examples in [1]. With the growing functionality and ubiquity of smartphones, athletes and coaches have access to an increasingly capable and sophisticated measurement system that includes the phone's inertial measurement unit (three dimensional angular rate gyroscope, accelerometer, and magnetometer) and determinants of location (GPS, GLONASS, etc.). Modern smartphone technology provides position measurements that can be sampled up to about 1 Hz with stationary absolute accuracy between 0.5 m to 16 m and stationary RMSE between 14 m to 71 m, making them more precise than accurate [2]. The phones also output acceleration and angular velocity data at rates up to about 200 Hz [3].

Competitive rowing attempts to maximize average boat speed over a specified race distance. For competitions over such a distance, the time domain race-to-race variability for elite rowers is approximately 1% and this has been proposed as "an irreducible error for any measure of rowing performance" [4]. However, the discrete unit of action and control in rowing is the stroke and this accordingly represents the domain in which many training and racing parameters are communicated and analyzed. For example, rowing speed is represented in the stroke domain as the product of stroke rate and distance per stroke.

In Olympic rowing races, the historical speed difference between finish position (first and second; second and third; etc.) has averaged 0.42% [5]. Contextualized in the approximately 200 strokes that it takes to complete a 2000 m race, rowers who generate an additional 5 cm per stroke will ordinarily gain a one place improvement in boat finish. Thus, it follows that the accuracy and precision of distance per stroke measurements must be better than 5 cm in order to generate meaningful insight and feedback. Satellite-based positioning systems (GPS, etc.) do not ordinarily afford this level of accuracy and precision thus limiting their effectiveness in the analysis of any individual stroke. We posit that more accurate and precise measures of boat movements for and within an individual stroke will enable a more direct examination of the causal relationships that exist between rower-oar-boat system mechanics and boat performance. Therefore this study seeks to improve the accuracy and precision of rowing metric measurements.

The paper begins with an explanation of the quality of the data available via the smartphone and the accuracy needs of the desired performance metrics. Two methods are then presented for fusing the smartphone position and motion data to generate more accurate position estimates. Finally, the estimates are presented relative to ground truth data collected from a differential GPS (DGPS) system. We close with discussion of the implications and use cases.

Related work

Real-time water-relative boat speed has traditionally been measured by either a pitot tube or a small impeller attached to the hull. More modern speedometers make use of GPS receivers to calculate Earth-relative speed and distance in the distance, time, and stroke domains. For example, the popular SpeedCoach GPS (Nielsen Kellerman, Boothwyn, PA, USA) outputs metrics like boat speed, stroke rate, distance, and elapsed time based on GPS and/or impeller measurements. The accuracy and utility of these systems are limited by the position estimation accuracy and/or the difficult-to-know and frequently fluctuating current velocity. GPS has been used to measure position during long distance (15,000 m) rowing events [6], and low cost GPS systems have also been shown to be capable of providing real-time speed estimates during rowing [7].

Other references exist to high accuracy ($0.1\,\mathrm{m\,s^{-1}}$ to $0.3\,\mathrm{m\,s^{-1}}$) GPS measurements for rowing [8] and the use of high accuracy differential GPS [9], but these systems are often impractical for ordinary rowing applications because they require establishing and operating an additional stationary base station. There has been success in creating differential GPS systems from a network of smartphones that improve location estimates to 1 cm accuracy at 1 Hz [10] that might be applicable to rowing. And a differential GPS-tailored Kalman filter has been used for the specific task of rowing position prediction [11].

Researchers have improved the accuracy of position and speed estimates in rowing by incorporating acceleration measures. Accelerometer-derived speed shows strong correlation to impeller-derived speed measurements in still water [12]. GPS and accelerometer sensor fusion have been used to estimate position and velocity during

GPS network downtime. References [13–15] compare GPS accelerometer-derived velocity to high speed video footage, and [16] measures differential GPS and acceleration showing the utility of advanced sensors.

A network of IMUs on the rower can capture rowing with similar results to motion capture cameras [17] and real-time accelerometer-based feedback has been found to improve rowing consistency when used on indoor ergometers [18]. Tessendorf et. al [19] use an elaborate IMU sensor array (Xsens, Enschede, Netherlands) to demonstrate the utility of metrics for characterizing on-water rowing performance but this system requires extensive setup time and expertise and is cost prohibitive for the typical rower. Various filters have been used to improve smartphone position estimates for walking in [20], but the large sensor error causes difficulties when applied to this more general problem.

Various methods have been proposed to improve measurement results during rowing. The most similar to the present paper is that of Hermsen [21], whose primary goal was to estimate the position, speed, and stroke rate of the boat based on a consumer-grade accelerometer and GPS sensor for real-time wireless transmission and display to viewers of the rowing event. His linear Kalman filter based approach fused data from the two sensors and estimated rowing speed. It found finish times to be 14% more accurate than when estimated with GPS data alone. Although real-time estimates were desired, the solution to handling sensor orientation bias required an offline after-the-fact computation leaving real-time implementation out of reach.

Problem Formulation

We desire highly accurate estimates of the distance the boat travels along its path during each individual stroke using readily available and easy to use consumer products, i.e., smartphones. High accuracy allows for intra-rower, -race, and -day repeatable comparisons in both distance traveled and boat speed. In competitive rowing, boats move on the order of 6 m per stroke. We have found smartphones to have raw accuracy on the order of 1 m and a precision of 0.8 m by comparison with our differential GPS measurements; see Table 1. Our ultimate goal is to improve this distance accuracy by roughly two orders of magnitude, allowing distance per stroke estimates with up to 5 cm accuracy. Additionally, we want these estimates to be able to be calculated in real time and not rely on knowledge of the specific boat and rower, to facilitate simple real-time training feedback to coaches and rowers. Our proposed methods to accomplish this consist of four major components:

Data collection A smartphone is rigidly attached to a boat and used to collect GPS data at an average sampling rate of 0.3 Hz and accelerometer data at approximately 100 Hz. (A differential GPS unit is also attached to the boat to measure boat position at 10 Hz for validation purposes, but this is not part of the evaluated method.)

Sensor fusion Physics-informed fusion of the raw GPS and accelerometer measurements to estimate position at the accelerometer sampling rate (100 Hz) .

Rowing metric computation Stroke transition detection is used to calculate the distance traveled per stroke, stroke rate, and boat speed.

Error estimates Estimates from the sensor fusion are compared to "true" values obtained from the differential GPS measurements.

Fig 1 provides a schematic of the general flow of data and processing algorithms from the prior list. The primary algorithm, i.e. transforming raw smartphone data to
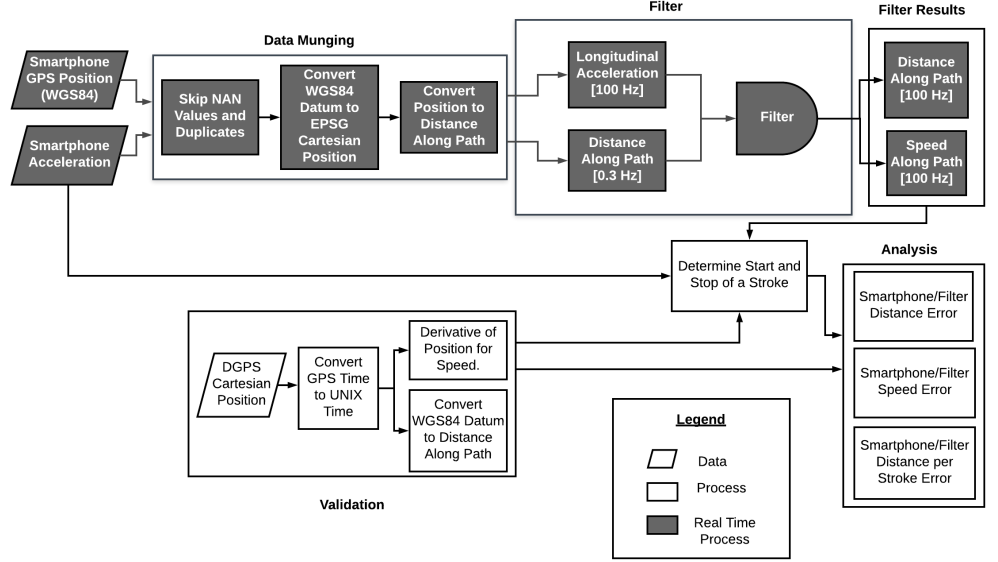
Fig 1. Data processing pipeline flow chart.
Grey rectangles indicate the real-time algorithm process. White rectangles indicate the validation process. Parallelograms represent raw data from the sensors.

distance and speed estimates, is implemented for use in a real-time computing situation, but the actual results for the purposes of the paper were computed offline and are available in the accompanying software. In this section we elaborate on the four components listed above, beginning with the characterization of the measurement data. We then motivate the desired accuracy of the metrics, and finally provide the details of the two sensor fusion methods.

Accuracy and precision

It is worth carefully defining accuracy and precision [2] of repeated measurements of a motionless sensor and of measurements while the sensor is moving.

Accuracy specifies how close a given measurement is to the true value. In the case of planar Cartesian horizontal position measurements (x, y) derived from latitude and longitude of a motionless sensor, following [2] we use the Central Error, CE, (i.e. Euclidean distance between the average of a set of measurements, $(\bar{x}, \bar{y})$, and the true position, (x_s, y_s), as a measure of accuracy.

$$\text{CE}_{xy}^2 = (\bar{x} - x_s)^2 + (\bar{y} - y_s)^2 = \left[\frac{1}{n}\sum_{i=1}^{n}(x_i - x_s)\right]^2 + \left[\frac{1}{n}\sum_{i=1}^{n}(y_i - y_s)\right]^2 \qquad (1)$$

Precision characterizes how repeatable measurements are [2]. For measurements from a motionless sensor the variance about the mean position in the Cartesian coordinates is a measure of precision, Eq (2).

$$\text{Var}(x) = \frac{1}{n}\sum_{i=1}^{n}(x_i - \bar{x})^2, \quad \text{Var}(y) = \frac{1}{n}\sum_{i=1}^{n}(y_i - \bar{y})^2 \qquad (2)$$

The Federal Geographic Data Committee recommends using the Root Mean Square Error (RMSE) to characterize error in geographic position measurements [2]. It is

important to note that RSME is related to both accuracy and precision. For example, increases in either the Central Error or the variance of the measurements will increase RMSE:

$$\text{RMSE}_{xy}^2 = \frac{1}{n}\sum_{i=1}^{n}\left[(x_i - x_s)^2 + (y_i - y_s)^2\right] = \text{CE}^2 + \frac{n-1}{n}\left[\text{Var}(x) + \text{Var}(y)\right] \quad (3)$$

We have elected to report RMSE values in this paper to follow this convention. We calculate the error between the smartphone measurements (or smartphone derived estimates) and the measurements from the differential GPS, which we define as the ground truth.

In this paper, we are primarily concerned with estimates of the distance and speed along the boat's nearly straight path during rowing. Here we define the accuracy and precision of these time varying estimates. We calculate this distance for the smartphone and DGPS at any given time with

$$d(t_i) = d(t_{i-1}) + \sqrt{[x(t_i) - x(t_{i-1})]^2 + [y(t_i) - y(t_{i-1})]^2}. \quad (4)$$

The boat speed is estimated from the DGPS data using a backward difference.

$$v_{\text{DGPS}}(t_i) = \frac{d(t_i) - d(t_{i-1})}{t_i - t_{i-1}} \quad (5)$$

Given the boat position and speed along the path we calculate the RMSE of the two prior quantities by comparing them with analogous quantities derived from the differential GPS data to quantify accuracy and precision (Eqs (6) and (7)). In this case n is taken as the number of samples associated with the larger sample rate of the two signals and linear interpolation is used to find corresponding samples in the signal with the smaller sample rate.

$$\text{RMSE}_d = \sqrt{\frac{\sum_{i=1}^{n} d_e(t_i)^2}{n}} = \sqrt{\frac{\sum_{i=1}^{n}[d(t_i) - d_{\text{DGPS}}(t_i)]^2}{n}} \quad (6)$$

$$\text{RMSE}_v = \sqrt{\frac{\sum_{i=1}^{n} v_e(t_i)^2}{n}} = \sqrt{\frac{\sum_{i=1}^{n}[v(t_i) - v_{\text{DGPS}}(t_i)]^2}{n}} \quad (7)$$

For given errors d_e and v_e at every time sample, the mean of the errors (Eqs (8) and (9)), and the variance of the errors, (Eqs (10) and (11)) can be computed.

$$\bar{d}_e = \frac{1}{n}\sum_{i=1}^{n} d_e(t_i) = \frac{1}{n}\sum_{i=1}^{n}[d(t_i) - d_{\text{DGPS}}(t_i)] \quad (8)$$

$$\bar{v}_e = \frac{1}{n}\sum_{i=1}^{n} v_e(t_i) = \frac{1}{n}\sum_{i=1}^{n}[v(t_i) - v_{\text{DGPS}}(t_i)] \quad (9)$$

$$\text{Var}(d_e) = \frac{1}{n}\sum_{i=1}^{n}[d_e(t_i) - \bar{d}_e]^2 \quad (10)$$

$$\text{Var}(v_e) = \frac{1}{n}\sum_{i=1}^{n}[v_e(t_i) - \bar{v}_e]^2 \quad (11)$$

The central error is then simply

$$\text{CE}_{d_e} = \sqrt{\bar{d}_e^2} = |\bar{d}_e|, \quad \text{CE}_{v_e} = \sqrt{\bar{v}_e^2} = |\bar{v}_e| \quad (12)$$

Table 1. Sensor measurement accuracy and precision.
The rows corresponding to the smartphone GPS provide the accuracy (central error,
CE) and precision (standard deviation, SD) of the GPS-derived position relative to
simultaneously collected DGPS position of the moving pair of sensors. The smartphone
accelerometer rows provide a measure of precision of the sensor's body fixed
acceleration when the smartphone is motionless. Similarly, the differential GPS rows
provide a measure of precision of the motionless rover position relative to the motionless
base station.

Sensor	Measurement	Value
Smartphone GPS (Moving, 32 sec)	CE of NS position	1.01 m
	CE of EW position	0.89 m
	SD in the NS position	0.81 m
	SD in the EW position	0.70 m
Smartphone Accelerometer (Motionless, 96 sec)	SD along the X axis	2.67 mg
	SD along the Y axis	2.45 mg
	SD along the Z axis	1.59 mg
Differential GPS (Motionless, 57 sec)	SD in the N-S position	3.2 mm
	SD in the E-W position	1.7 mm

The RMSE is related to the mean and variance [2]

$$\mathrm{RMSE}_d^2 = \mathrm{CE}_{d_e}^2 + \mathrm{Var}(d_e), \quad \mathrm{RMSE}_v^2 = \mathrm{CE}_{v_e}^2 + \mathrm{Var}(v_e) \tag{13}$$

Lastly, we calculate the RMSE of the actual distance per stroke relative to the
estimated distance per stroke for all strokes, or subsets of strokes.

$$\mathrm{RMSE}_{d_s} = \sqrt{\frac{\sum_{i=1}^{m}[d_{si} - d_{\mathrm{DGPS}si}]^2}{m}} \tag{14}$$

where d_s is the distance per stroke and m is the number of strokes. ₁₃₅

Data collection ₁₃₆

Smartphone GPS ₁₃₇

The smartphone provides global position estimates accessed via the iPhone software ₁₃₈
development kit. Latitude and longitude are received at a variable sampling rate, 0.1 Hz ₁₃₉
to 1 Hz, usually at an average of about 0.3 Hz when the sensor is in motion. Once the ₁₄₀
data is transformed into an Earth-local Cartesian coordinate system with respect to the ₁₄₁
WGS84 coordinate system [22], the precision of motionless measurements can be ₁₄₂
determined; see Table 1. For repeated measurements over a short duration (<15 min) ₁₄₃
we assume that any inherent systematic bias of the GPS relative to true position is ₁₄₄
constant and does not degrade our distance calculations. Systematic bias can be quite ₁₄₅
large, e.g. 16 m, but the precision of repeated measurements over a short duration can ₁₄₆
be at least an order of magnitude smaller [2]. ₁₄₇
None of the metrics of interest we describe in the prior section requires knowledge of ₁₄₈
the absolute position of the boat on the earth; instead we require only relative ₁₄₉
sample-to-sample (x, y) position differences. Using a Piksi differential GPS system ₁₅₀
(SwiftNav, San Francisco, USA) as a measure of ground truth relative position (with ₁₅₁
better than 1 cm precision) we characterized the motionless and moving ₁₅₂
mean-subtracted distribution of smartphone position measurements; see Table 1. ₁₅₃
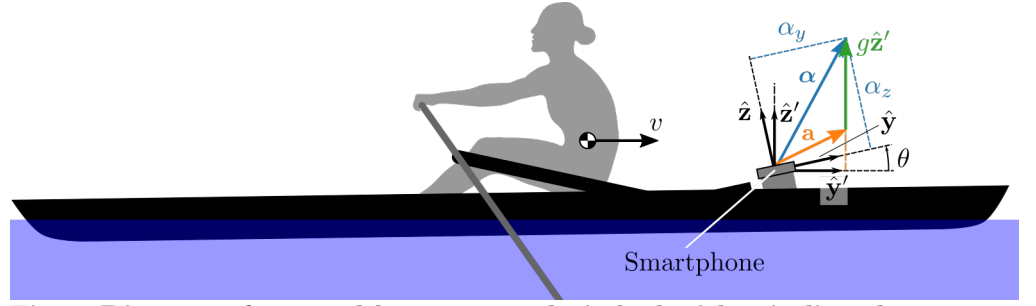
Fig 2. Diagram of a rowed boat at speed pitched with misaligned bow-mounted smartphone.
The smartphone coordinate system $\hat{\mathbf{y}}, \hat{\mathbf{z}}$ is oriented relative to the coordinate system aligned with the horizontal $\hat{\mathbf{y}}', \hat{\mathbf{z}}'$ by the varying pitch angle θ. The accelerometer-reported acceleration $\boldsymbol{\alpha}$ differs from the actual $\hat{\mathbf{y}}'$ component because it includes a gravitational component. The actual acceleration $\mathbf{a}$ of the phone is then $\mathbf{a} = \boldsymbol{\alpha} - g\hat{\mathbf{z}}'$. We desire the magnitude of the acceleration $\mathbf{a}$ projected onto the horizontal plane but we do not know θ at any given time. As described in the text, the sensed $\hat{\mathbf{y}}$ acceleration differs from the true $\hat{\mathbf{y}}'$ acceleration by a small bias and a larger term $g\theta$ which accounts for the projection of the gravity vector on the pitched $\hat{\mathbf{y}}$ axis.

The cumulative distance traveled along the boat's path is calculated from the relative distance between each (x, y) coordinate; see Eq (4). We rely on numerical differentiation (backward differences, see Eq (5)) with respect to the sensor-recorded time stamps to compute speed from the DGPS position measurements.

Smartphone acceleration

The smartphone accelerometer provides three dimensional body-fixed acceleration measurements with a precision (SD) of about $0.02\ \mathrm{m\,s^{-2}}$, Table 1, updated at approximately 100 Hz. When affixed to the boat, we are interested in the component of acceleration tangent to the boat's travel path on the water surface.

The very small yaw ($<1°$) angular motion during typical rowing [5] allows us to ignore the lateral acceleration component. We also ignore effects of any boat rolling motion, because it is small as well [5]. Pitch angular motion is similarly small (<1 °) [5] but because of the relatively large gravitational acceleration, even small changes in pitch mounting orientation, average boat pitch, and time-varying pitch angle mean that the longitudinal smartphone acceleration measurement cannot be used directly; see Fig 2.

In general, we use only the smartphone-fixed longitudinal component of acceleration, α_y to estimate distance, but must take special care to account for the pitch effects and accumulation of error from twice integrating the biased accelerometer measurement. Although this could be corrected by a calibration procedure [21], it is generally not practical in the expected smartphone consumer use case. Fig 2 illustrates how the smartphone body-fixed sensed acceleration relates to the actual acceleration parallel to the water's surface. If the smartphone pitch, θ, and the vertical acceleration of the boat are small, then the longitudinal acceleration follows

$$a \approx \alpha_y - g\theta. \tag{15}$$
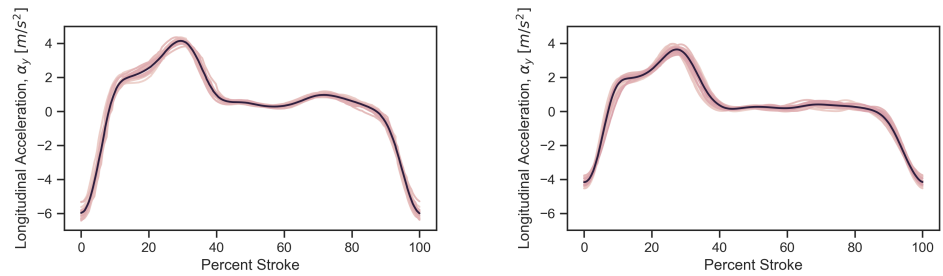
(a) Elite rower   **(b)** Club-level rower

Fig 3. Boat-fixed longitudinal acceleration as a function of percent stroke from two trials (elite and club-level 24SE.).
Each stroke is plotted as a red line and the mean of all strokes as a black line. The repeatability of the measured longitudinal acceleration, especially for the elite rower, lends credence to the consistency of both rowing technique, the robustness of the stroke endpoint identification, and the quality of the data itself.

Desired Kinematic Metrics

Stroke rate

Rowing involves periodic propulsive strokes by the rower(s) delivered through the oars to generate boat movement. These create a periodic kinematic pattern of boat accelerations and pitching that reliably maps to the characteristic phases of the stroke. Similar to others [14], we defined the endpoints of the stroke (the end of one and start of the next) as the time that corresponds to the minimum peak values of longitudinal boat acceleration. This moment reliably corresponds to the beginning of propulsive phase of the stroke, commonly referenced in rowing as the "catch" [5]. These time instants can be detected in real-time using the method from [23], for example. Fig 3 illustrates the reliability of individual stroke endpoints detected using this method. These times are used to calculate the stroke-domain metrics of interest: distance per stroke and stroke rate.

Boat speed

Average boat speed along the shortest path to the finish is the primary metric rowers must maximize to win a race. We compute boat speed for the differential GPS measurements using Eq (5), and for the smartphone we rely on its internal speed estimate directly. Fig 4 provides a look at the DGPS computed speed measures for two trials.

Determining instantaneous earth-relative boat speed relies on accurate distance estimates. The smartphone provides a low accuracy and reasonable precision position update at a sample rate on the same order of magnitude as the stroke rate, i.e. 0.3 Hz, which is only useful for average speed estimates for a given stroke.

Given a 0.8m precision in the distance measurements (Table 1), the accuracy of the speed estimates from the phone are on the order of 0.3 m s^{-1}. With a 5 cm precision, the accuracy can potentially increase to 0.02 m s^{-1}, thus providing an intimate view of intra-stroke speed variations.
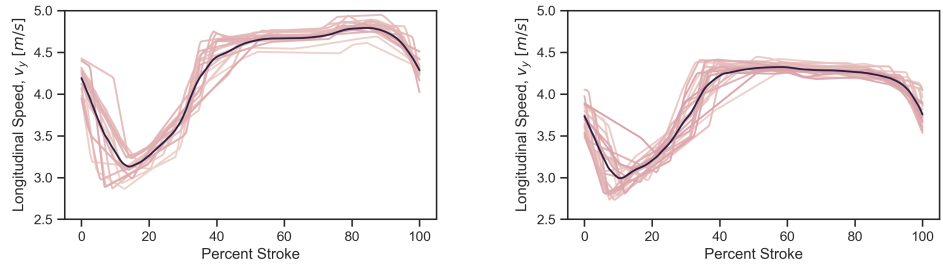
Distance per stroke

Boat speed is the product of two separate but interrelated variables in the stroke domain: stroke rate and distance per stroke. We calculate distance per stroke for each

(a) Elite rower　　　　　　　　　　　　**(b)** Club-level rower

Fig 4. DGPS computed boat speed as a function of percent stroke for two trials (elite and club-level 24SE).
Each stroke is plotted as a red line and the mean of all strokes as a black line. Because the DGPS data is sampled at only 10 Hz and the relative precision is lower than the accelerometer, the speed profile is less smooth and repeatable than the acceleration profiles in Fig 3.

Table 2. Summary DGPS stroke data from the elite 24SE trial
Same data as depicted in Figs 3 and 4.

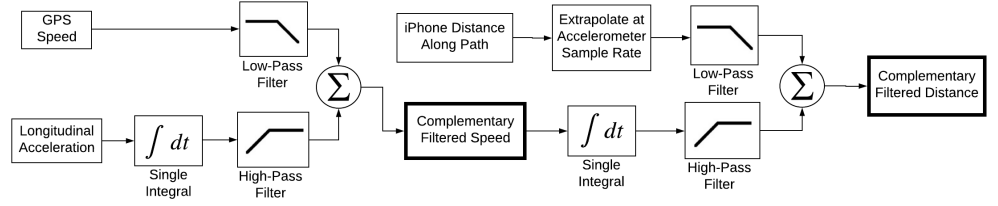| Stroke Number	Duration [s]	Distance [m]	Avg. Speed [$\mathrm{m\,s^{-1}}$]
1	2.52	10.10	4.03
2	2.48	10.10	4.05
3	2.37	9.89	4.15
4	2.36	9.98	4.18
5	2.35	10.03	4.26
6	2.31	9.79	4.27
7	2.29	9.89	4.32
8	2.33	10.06	4.30
9	2.25	9.59	4.22
10	2.28	9.84	4.39
11	2.28	9.89	4.36
12	2.43	10.52	4.36
13	2.41	10.36	4.26
14	2.40	10.27	4.34
15	2.39	10.21	4.32
16	2.42	10.20	4.24
17	2.37	9.98	4.20
18	2.38	10.09	4.24
19	2.34	9.95	4.20
20	2.33	9.66	4.16
AVG	2.36	10.02	4.24
STD	0.07	0.23	0.10

Table 3. Summary DGPS stroke data from the club-level 24SE trial
Same data as depicted in Figs 3 and 4.

Stroke Label	Duration [s]	Distance [m]	Avg. Speed [$\mathrm{m\,s^{-1}}$]
1	2.50	9.80	3.90
2	2.43	9.43	3.80
3	2.44	9.71	3.98
4	2.37	9.49	4.02
5	2.52	10.02	3.93
6	2.62	10.28	3.95
7	2.37	9.42	3.95
8	2.41	9.59	3.99
9	2.49	9.82	3.91
10	2.49	9.84	3.86
11	2.47	9.63	3.90
12	2.37	9.32	3.95
13	2.57	10.07	3.90
14	2.44	9.66	3.93
15	2.61	10.34	3.97
16	2.43	9.47	3.93
17	2.47	9.76	3.92
18	2.46	9.68	3.96
19	2.46	9.56	3.86
20	2.56	9.98	3.92
21	2.42	9.34	3.91
22	2.43	9.54	3.97
23	2.46	9.62	3.93
24	2.44	9.30	3.78
AVG	2.46	9.69	3.92
STD	0.07	0.29	0.05

Table 4. Summary DGPS data for strokes from the elite and club-level 24SE trials

Same data as depicted in Figs 3 and 4.

Stroke Number	Duration [s]	Distance [m]	Avg. Speed [$\mathrm{m\,s^{-1}}$]
1	2.52	10.10	4.03
2	2.48	10.10	4.05
3	2.37	9.89	4.15
4	2.36	9.98	4.18
5	2.35	10.03	4.26
6	2.31	9.79	4.27
7	2.29	9.89	4.32
8	2.33	10.06	4.30
9	2.25	9.59	4.22
10	2.28	9.84	4.39
11	2.28	9.89	4.36
12	2.43	10.52	4.36
13	2.41	10.36	4.26
14	2.40	10.27	4.34
15	2.39	10.21	4.32
16	2.42	10.20	4.24
17	2.37	9.98	4.20
18	2.38	10.09	4.24
19	2.34	9.95	4.20
20	2.33	9.66	4.16
AVG	2.36	10.02	4.24
STD	0.07	0.23	0.10

Fig 5. Block diagram depicting the complementary filter algorithm.
The smartphone speed and acceleration are fused to create an improved speed estimate
and then that estimate is fused with the smartphone GPS-derived distance to create an
improved distance estimate.

stroke by subtracting the interpolated distance, Eq (4), at each pair of subsequent   200
stroke start/stop times. The same synchronized start/end time values are used for the   201
smartphone-derived and reference differential GPS data allowing a direct comparison of   202
the various estimations of boat distance. This comparison will provide an estimate of   203
the accuracy and precision of each estimate method presented below.   204

As another indication of the effectiveness of the stroke endpoint identification   205
procedure and the subsequent calculations of stroke time, distance per stroke and   206
average speed, Tables 4 and 3 provide statistics on the apparently repeatable strokes   207
contained in the two trials portrayed in Figs 3 and 4. The deviations of the duration   208
and distance of each stroke are of the order of 2-3%, which means that the rowers were   209
rowing steadily and that the stroke endpoint identification procedure and subsequent   210
calculation of the stroke parameters from the DGPS data is robust.   211

Sensor Fusion Method 1: Complementary Filter   212

The first method stems from the classical idea of characterizing input-output behavior   213
based on frequency response. We utilize two complementary filters in series, Fig 5, with 214
each filter made up of two real-time discrete 2$^{\text{nd}}$ order Butterworth filters, one low-pass   215
presented in [24] and one high-pass of similar design. Integrating the biased and noisy   216
acceleration measurement introduces drift in the speed and distance estimates, as   217
expected. The high-pass filter is used to extract the high frequency portion of the   218
estimates and to exclude the low frequency drift component. The low-pass filter extracts 219
the low frequency portion of the smartphone speed and GPS-derived distance estimates.   220
Each pair of two filtered signals are then summed at each accelerometer sample time to   221
update the estimates. The result is a more accurate speed and distance estimate.   222

Extrapolating GPS data   223

Since the GPS measurements are updated less frequently than the accelerometer
measurements, the smartphone speed and GPS-derived distance is linearly extrapolated,
Eq (16), between GPS updates at each accelerometer update. This uses the prior two
GPS samples to provide an often improved complementary filter input. This simple
additional "filtering" technique improves the distance estimate by 37% and the velocity
estimate by 20%. In the below equation the i index represents the accelerometer update
time and the k index represents the last GPS update prior to t_i. This amounts to using
the average speed derived from the GPS to make the extrapolation.

$$d(t_i) = d(t_{i-1}) + \frac{d(t_k) - d(t_{k-1})}{t_k - t_{k-1}}(t_i - t_{i-1}) \tag{16}$$

Table 5. Average optimal Butterworth filter cutoff frequencies.

Distance Filter		Speed Filter	
low [Hz]	high [Hz]	low [Hz]	high [Hz]
0.189	3.789	0.0166	0.0457

Cutoff Frequency Selection

A unique cutoff frequency is computed for each filter (low-pass and high-pass) for each trial. We select these parameters using an offline nonlinear least squares curve fit comparing the filtered distance to the differential GPS distance to compute the error. These optimal cutoff frequencies are averaged across all trials and the result is used in the real-time implementation. See Table 5.

Using the optimal cutoff frequency for each pass as opposed to the average over all passes would decrease the position RMSE by an average of 26% and the velocity RMSE by an average of 16%. However, calculating optimal cutoff frequencies would require post-processing and would render this filter non-real time.

Bias and the Butterworth Filter

A Butterworth filter creates a maximally flat passband and is relatively easy to implement digitally. At the cutoff frequency it rolls off gradually but is sufficient for many biomechanical filtering needs [1]. The transfer functions for the low and high pass 2nd Butterworth filters are shown in Eqs (17) and (18) alongside the equations for the magnitude in the frequency domain.

$$H_{\text{low}}(s) = \frac{\omega_c}{s^2 + \sqrt{2}\omega_c s + \omega_c}, \quad |H_{\text{low}}(j\omega)| = \frac{1}{\sqrt{1 + \left(\frac{\omega}{\omega_c}\right)^4}} \tag{17}$$

$$H_{\text{high}}(s) = \frac{s^2}{s^2 + \sqrt{2}\omega_c s + \omega_c}, \quad |H_{\text{high}}(j\omega)| = \frac{1}{\sqrt{1 + \left(\frac{\omega_c}{\omega}\right)^4}} \tag{18}$$

We low pass filter the smartphone GPS speed estimate and high pass filter the longitudinal accelerometer measurement. The accelerometer output is the sum of the acceleration along the travel path minus a term that varies with boat pitch about a constant bias, i.e. $\alpha_y - g\theta$. In the frequency domain, these two signals are

$$X_{\text{low}}(j\omega) = V(j\omega) \tag{19}$$

$$X_{\text{high}}(j\omega) = A(j\omega) + a_0 \tag{20}$$

where a_0 represents the bias.

Once filtered, the magnitude of each signal becomes

$$|Y_{low}(jw)| = \frac{V(jw)}{\sqrt{1 + (\frac{w}{w_c})^4}} \tag{21}$$

$$|Y_{high}(jw)| = \frac{|A(jw)|}{\sqrt{1 + (\frac{w_c}{w})^4}} + \frac{a_0}{\sqrt{1 + (\frac{w_c}{w})^4}} \tag{22}$$

$$\tag{23}$$

The low-pass filter can be tuned with the cutoff frequency. However, the high-pass cutoff frequency must be tuned to maximize the expression of the non-bias term and to

minimize the expression of the bias term in the output. If the bias term has frequency content in the same bandwidth as desirable signal in the non-bias term it is difficult to separate. Because the bias term and the longitudinal acceleration both vary with the boat pitch, this the filter may not be ideal, but in practice performance is sufficient. The Kalman filter described in the next section, on the other hand, does not have this limitation.

Sensor Fusion Method 2: Kalman filter

The Kalman filter algorithm fuses data collected from different sensors with the outputs of a predictive dynamic physical model to estimate the target time-varying variables of interest, known as states. The estimation results are expected to be more accurate than those obtained from any individual sensor [25]. Although the Kalman filter formalism makes several foundational mathematical assumptions, perhaps the most important of which are random Gaussian process and measurement noise, these assumptions are often relaxed in practice and the technique still works [26].

In our case, the body-fixed longitudinal acceleration of the boat is measured and used as an input to a kinematic model to predict the displacement and speed of the boat along its path. The predictions are then compared with the smartphone GPS-derived distance traveled and speed measurement and the error is used as feedback to adjust the estimation in real time. The Kalman gain can be tuned to balance the sensor and model uncertainty to achieve optimal accuracy. Details regarding the application of Kalman filtering to this estimation problem will be discussed in this section.

Boat Kinematic Model

The Kalman filter uses a discrete dynamic model describing the kinematic relationships along the path. The actual horizontal acceleration a is discretely twice integrated to obtain distance d and speed v,

$$d_{k+1} = d_k + v_k \Delta t. \tag{24}$$

$$v_{k+1} = v_k + a_k \Delta t \tag{25}$$

where the subscripts are shorthand for $d_k = d(t_k)$, etc.

As noted previously and illustrated in Fig 2, the smartphone's y accelerometer axis is not, in general, parallel to the boat's horizontal travel path. If we want to use the smartphone acceleration for a in Eq (25) above, we must compensate for this misalignment together with varying boat pitch during rowing by adjusting the accelerometer's reading. We introduce an unknown constant bias state, ϕ_k for this purpose

$$\phi_{k+1} = \phi_k \tag{26}$$

and replace a with $\alpha_{y,k} - \phi_k$, where ϕ_k is essentially the sum of the real accelerometer bias and the mean of $g\theta(t)$. The augmented speed state equation follows in Eq. (27).

$$v_{k+1} = v_k + (\alpha_{y,k} - \phi_k)\Delta t. \tag{27}$$

This bias can be thought of as the "effective" bias, in that it is the sum of the "real" bias and the mean value of $g\theta$ and has now become a new state to be estimated by the filter which will effectively account for drift due to integration error accumulation. The time varying component of $g\theta(t)$ is the sum of two parts: a roughly periodic remnant and a small truly random measurement noise. These two parts are luped together as "process noise" $\mathbf{w}_k$ below.

Lastly, we make use of two measurements, d and v, which is the smartphone GPS derived distance and speed along the travel path to correct our kinematic model predictions. Eqs (24) and (27) can be written in state space form to facilitate the design of the filter.

$$\mathbf{x}_{k+1} = \mathbf{A}\mathbf{x}_k + \mathbf{B}\mathbf{u}_k + \mathbf{w}_k \tag{28}$$

$$\mathbf{y}_k = \mathbf{C}\mathbf{x}_k + \mathbf{D}\mathbf{u}_k + \boldsymbol{\nu}_k \tag{29}$$

where

$$\mathbf{x}_k = [d_k, v_k, \phi_k]^T, \quad \mathbf{u}_k = [\alpha_{y,k}], \quad \mathbf{y}_k = [d_k, v_k]^T, \tag{30}$$

and

$$\mathbf{A} = \begin{bmatrix} 1 & \Delta t & 0 \\ 0 & 1 & -\Delta t \\ 0 & 0 & 1 \end{bmatrix}, \quad \mathbf{B} = \begin{bmatrix} 0 \\ \Delta t \\ 0 \end{bmatrix}, \quad \mathbf{C} = \begin{bmatrix} 1 & 0 & 0 \\ 0 & 1 & 0 \end{bmatrix}, \quad \mathbf{D} = \begin{bmatrix} 0 \\ 0 \end{bmatrix}. \tag{31}$$

The terms $\mathbf{w}_k$ and $\boldsymbol{\nu}_k$ are the process and measurement noise representing model and sensor uncertainty, respectively.

Kalman filter formulation

Based on the state space model of the boat kinematics, we design a Kalman filter to estimate the states $\mathbf{x}_k$ over time. The Kalman filter generates the estimates in two steps: the model prediction update and the measurement update. In the prediction update, an *a priori* estimate is made based on the input, the estimated state at the previous time instant, and the model,

$$\hat{\mathbf{x}}_k^- = \mathbf{A}\hat{\mathbf{x}}_{k-1}^+ + \mathbf{B}\mathbf{u}_{k-1}, \tag{32}$$

where the superscript $^-$ denotes the *a priori* estimate and $^+$ denotes the final (*a posteriori*) estimate. In our case, the acceleration measurement is fed as the input to the kinematic model to calculate the instantaneous speed and distance. Meanwhile, the Kalman filter provides an estimate of the covariance of the state estimation, P, according to

$$\mathbf{P}_k^- = \mathbf{A}_{k-1}\mathbf{P}^+{}_{k-1}\mathbf{A}_{k-1}^T + \mathbf{Q}, \tag{33}$$

which indicates the estimation accuracy. In Eq (33), $\mathbf{Q}$ is the estimated covariance matrix of the process noise $\mathbf{w}_k$.

In the measurement update step, an *a posteriori* estimate is made based on the model prediction and the output measurement feedback,

$$\hat{\mathbf{x}}_k^+ = \hat{\mathbf{x}}_k^- + \mathbf{L}_k(\mathbf{y}_k - \hat{\mathbf{y}}_k^-) \tag{34}$$

$$\hat{\mathbf{y}}_k^- = \mathbf{C}_k\hat{\mathbf{x}}_k^- + \mathbf{D}_k\mathbf{u}_k, \tag{35}$$

where $\mathbf{L}_k$ is the Kalman gain matrix calculated as

$$\mathbf{L}_k = \mathbf{P}_k^- \mathbf{C}_k^T (\mathbf{C}_k \mathbf{P}_k^- \mathbf{C}_k^T + \mathbf{R})^{-1}. \tag{36}$$

In Eq (36), $\mathbf{R}$ is the covariance of the output measurement noise $\boldsymbol{\nu}_k$. During this step, the estimation covariance is also updated

$$\mathbf{P}_k^+ = (1 - \mathbf{L}_K \mathbf{C}_k^T)\mathbf{P}_k^-. \tag{37}$$

If both the process noise $\mathbf{w}_k$ and measurement noise $\boldsymbol{\nu}_k$ are Gaussian, the *a posteriori* estimate obtained in Eq (35) is optimal in the sense of minimum covariance $\mathbf{P}$. In our case, the smartphone GPS derived distance measurement is used to compare with and correct the *a priori* estimate of the boat distance and speed.

The model prediction is performed at approximately 100 Hz in accordance with the sampling rate of the accelerometer, while the measurement update is carried out at the less frequent update rate of the GPS, about 0.3 Hz.

The performance of the Kalman filter relies heavily on the filter designer's choice of values for the Q and R matrices. The correct values for both are difficult, if not sometimes impossible, to know, and the noise is often not actually Gaussian. But in practice, these can often be tuned to create a good estimate. We are able to directly calculate the smartphone measurement variance, taking the DGPS measurements as the true value, see Eqs (10) and (11) and we use it to populate the diagonals of $\mathbf{R}$.

$$\mathbf{R} = \begin{bmatrix} 25.279 & 0 \\ 0 & 0.309 \end{bmatrix} \tag{38}$$

Our process model is a simple kinematic model and the only terms that may have appreciable process noise are the acceleration input and the bias. We assume that the process noise is negligible because of the quality of the acceleration measurement and the dominance of the bias term in the development of error in the estimate. We thus, set $\mathbf{Q} = \mathbf{0}$, to reflect this and the filter trusts the model fully when no measurements are available. The values for $\mathbf{Q}$ and $\mathbf{R}$ are generally robust with respect to rower and boat variation.

Experimental Methodology

Experiments were performed two days apart to validate the effectiveness of the proposed sensor fusion methods using a different rower-boat combination on each day: an experienced club-level (18 years rowing experience, age=63, height=1.68 m, weight=70 kg) sculling a 2 person boat (2002 Hudson mid-weight, 2X) alone, and an elite rower (2016 Olympic participant, age=31 height=2.00 m, weight=100 kg) sculling a single person boat (2004 Hudson heavy-weight, 1X). The 2X boat was used with a single rower to allow for easy mounting of the measurement equipment to the empty aft seat before a mounting option for the single scull was developed. In each experiment, the rower performed a series of trials (each over a distance of approximately 300 m) in the West Sacramento channel in both the northwest and southeast directions(Fig 6). A SpeedCoach GPS (Model 2, Nielson-Kellerman, Boothwyn, PA) was used onboard to display to the rower their current stroke rate. An example trial path is shown in Fig 6.

An iPhone 7 smartphone with iOS 11.3 (Apple, Cupertino, USA) running a custom data-logger app SwingRow 1.1 (Hegemony Technologies, Davis, CA) was rigidly attached to the deck of the 1X boat using Dual Lock positive-locking fasteners (3M, St. Paul, MN) at the position and orientation shown in Fig 7. A second smartphone running the same data-logger app was put into a "rowers wallet" (Hegemony Technologies, Davis, CA), positioned flat against the back of the rower at the top of the pelvis, and worn throughout the experiments. A HERO4 Session camera (GoPro, San Mateo, USA) was mounted to stern hull facing the rower to collect video. A Piksi differential GPS roving antenna (Swiftnav, San Francisco, USA) was also attached to the hull as shown in Fig 7 (or in the spare seat in the case of the 2X boat).

Each rower performed a series of trials at different target stroke rates and in different directions. The current in the channel was investigated and found to be negligible. This data is available in the supplementary materials.

Fig 6. Satellite image of Washington Lake in West Sacramento, CA, USA showing the path of one of the trials.
The single red dot on the shore is the location of the DGPS base station. The mean latitude and longitude are 38.566435 ° and -121.556365 °, respectively.

Fig 7. Sensor locations during the elite experiments.
2004 Hudson heavy-weight rowed by elite rower, annotated with hardware used in the experiment and with DGPS antenna clearly visible to the sky (15 degrees from horizontal in all directions has clear view to the sky).
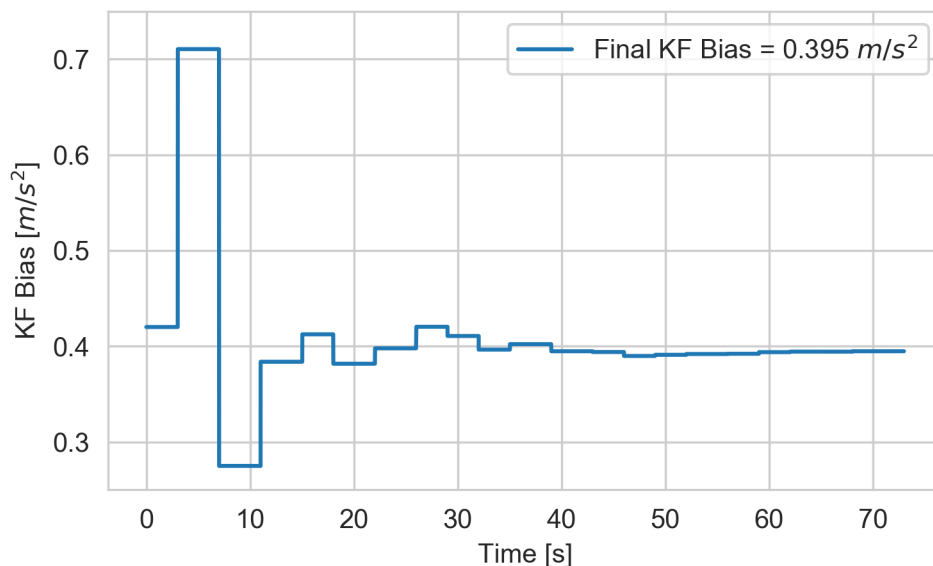
Fig 8. Convergence of the Kalman filter bias state over a single trial (elite 16NW).
The filter bias state typically takes about 40 seconds to converge to a relatively constant value.

Results

We used the GPS satellite-reported time to synchronize the measurements between the devices and to calculate the distance, speed, stroke rate, and distance per stroke from the smartphone and the differential GPS position data. The smartphone data was also used to calculate the estimates using the two aforementioned filters. This section reports the resulting comparisons among the four different estimates of each of the variables. A description of the detailed analysis procedure can be found in the accompanying software.

Filter convergence

The Kalman filter's performance relies on the effective bias ϕ converging to a constant value. Fig 8 shows ϕ as a function of time for a single example trial. In this case it takes almost 50 seconds (or 14 strokes) for convergence, which is nearly two thirds of the length of the trial. For this reason we limited the calculation of steady state performance data (RMSE) to the last ten strokes of each trial.

The filter converges on a different value of ϕ for each rower-boat combination and stroke rate. Fig 9 shows the steady state values of ϕ for every trial. This value increases with stroke rate as does the average boat pitch angle.

Distance estimates

Fig 10 shows all of the distance estimates and Fig 11 shows the relative error of the distance estimates with respect to the differential GPS derived distance from a single trial after filter convergence, see the prior section for an explanation of filter convergence. The Kalman filter estimate is similar to the smartphone, but provides a reasonably drift free estimate between adjacent smartphone updates. The
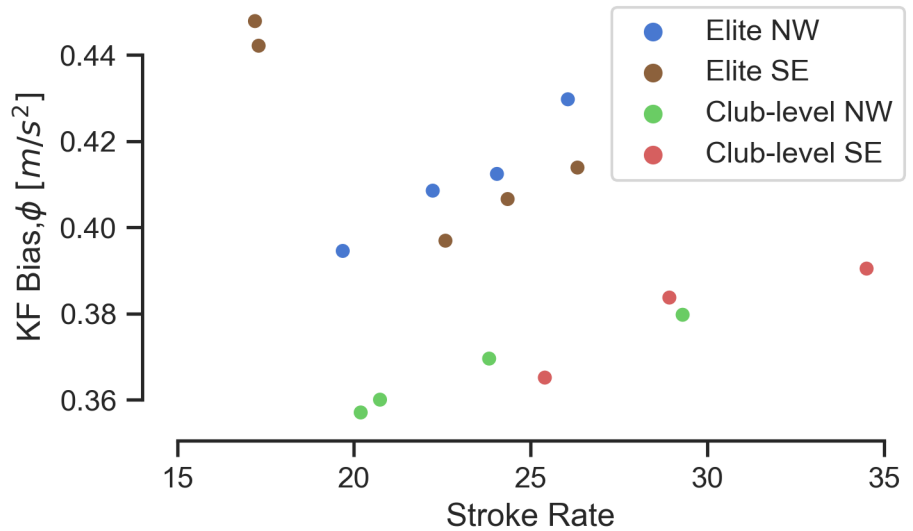
Fig 9. Terminal values of the Kalman filter bias state, ϕ_k, for each trial.
Each dot represents a single trial at the specified target stroke rate. The bias is dictated
by the rower/boat combination and the boat speed.

complementary filter is less influenced by the smartphone distance measurements and   346
provides a better estimate of the true distance traveled.   347

Fig 12 shows the distribution of RMSE for the distance estimates relative to the   348
DGPS for all trials for the elite and club-level rowers. The complementary filter shows   349
improvement for the club-level rower, but little improvement is seen for any of the other   350
cases relative to the smartphone. The Kalman filter actually is over a meter worse when   351
comparing the medians. The large RMSE for the filters is largely due to the bias in the   352
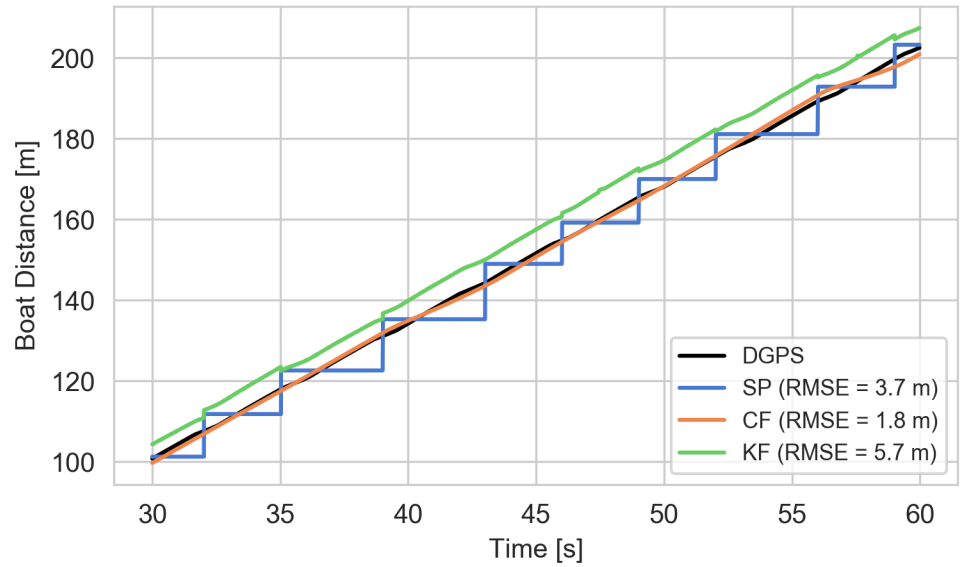estimate.   353

Boat speed estimates   354

Fig 13 shows example speed estimations from both the complementary and Kalman   355
filters after convergence compared to those derived from the raw smartphone GPS and   356
the differential GPS measurements for a typical trial. The RMSE of the estimations   357
with respect to the differential GPS are tabulated for the post-convergence portion of   358
time and shown on the graph for that trial. Both filters track the differential GPS   359
derived speed throughout the stroke much more closely than the smartphone GPS   360
derived speed, which is more like an average speed. Both of the filters improve the   361
estimate by over a factor of 2 in this trial.   362

Fig 14 shows the summary of the calculated RMSE values for each rower. It is clear   363
that both of the filters improve the speed estimates, also by about a factor 2 or more   364
when comparing the medians.   365

Distance per stroke estimates   366

Fig 15 compares the distance per stroke estimation computed from the smartphone,   367
complementary filter, and Kalman filter through the relative error with respect to the   368
the distance per stroke computed from the differential GPS measurements. For the   369
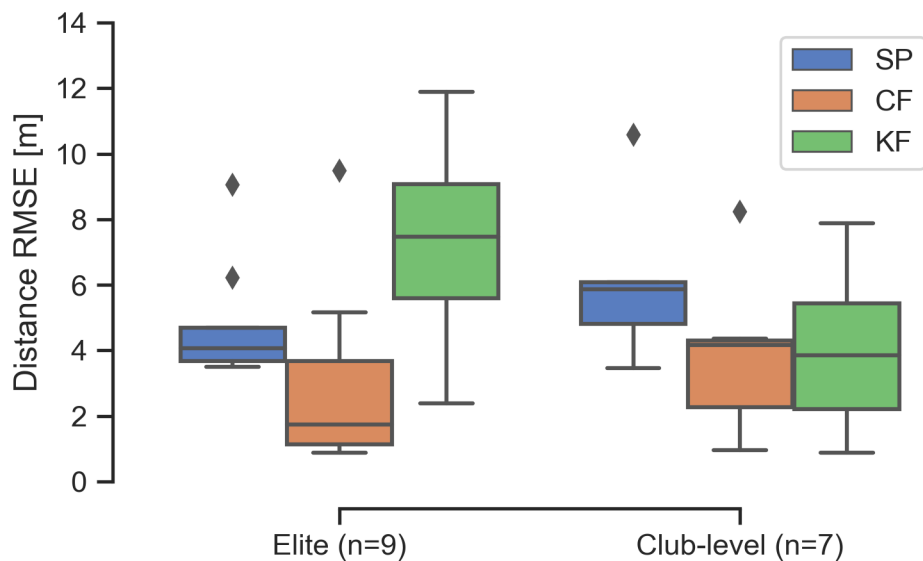
Fig 10. Example boat distance estimates.
The figure indicates the distance traveled as a function of time for the last 30 s of the elite 16NW trial as estimated by the smartphone, complementary filter, and Kalman filter. The reported RMSE values are with respect to the DGPS distance shown in black. Each RMSE is calculated with at the sampling rate of the accelerometer, i.e. approximately 100 Hz.
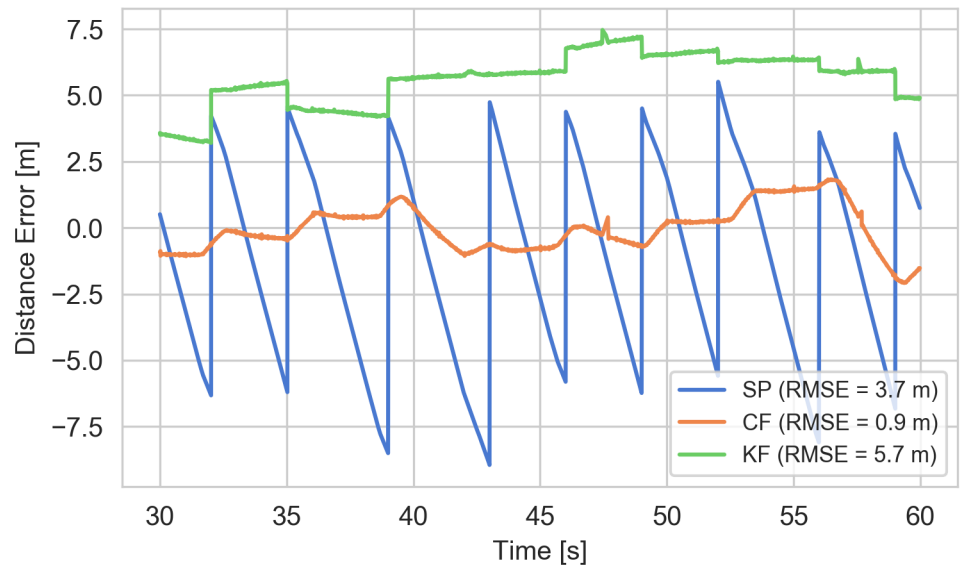

Fig 11. Example boat distance estimate error.
Error in the smartphone, complementary filter, and Kalman filter estimates relative to the DGPS. The smartphone error is based on the piece-wise constant curve shown in Fig 10 to highlight the issue it poses when one desires to calculate distance per stroke.

Fig 12. Summary of the distance estimate error for all trials.
Comparisons of the distributions of RMSE_d of the distance estimates from the three methods for each full length trial.
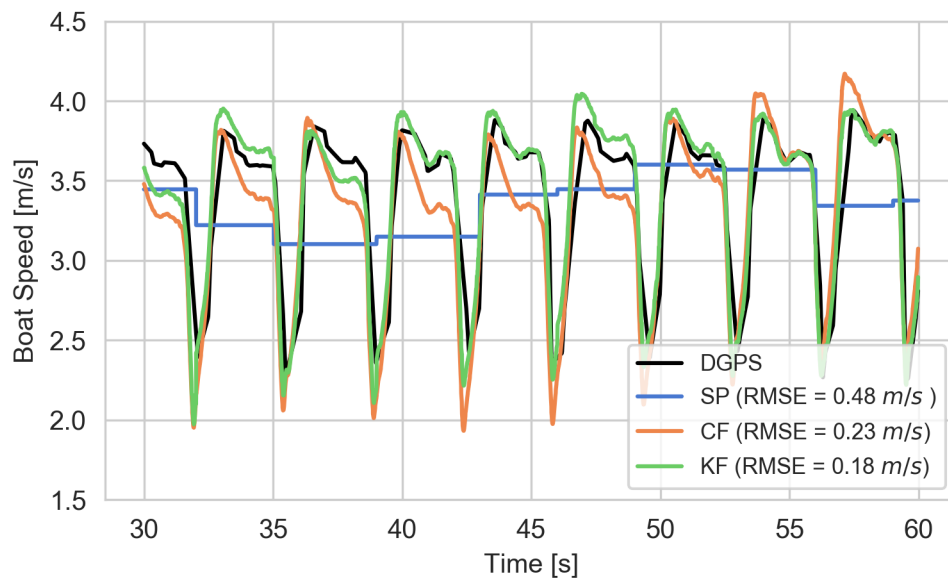
Fig 13. Example boat speed estimates.
The figure indicates the speed as a function of time for the last 30 s of the elite 16NW trial as estimated by the smartphone, complementary filter, and Kalman filter. The reported RMSE values are with respect to the DGPS computed speed shown in black. Each $RMSE_v$ is calculated at the sampling rate of the accelerometer, i.e. approximately 100 Hz.

Fig 14. Summary of the speed estimate error for all trials.
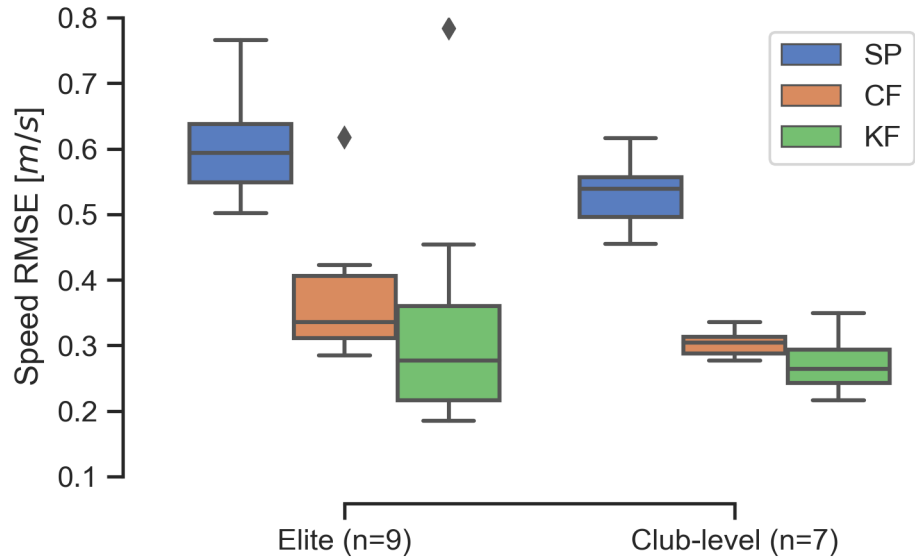Comparisons of the distributions of RMSE_v of the speed estimates from the three methods for each full length trial.

group of strokes that make up this trial we see that we obtain a ?× improvement and?×   370
improvement over the smartphone data alone. For this trial, the mean accuracy of this   371
estimation is x m.   372

Discussion   373

Rowing research, training, and racing methodologies are necessarily linked to the   374
accuracy and precision of the available measurement systems. Location-based solutions   375
like GPS make it possible to derive and report speed and related metrics in the stroke   376
domain, e.g., stroke rate and distance per stroke. However, efforts to monitor and effect   377
meaningful elite-level race result changes to these metrics at an individual stroke level   378
were shown in the introduction to require location accuracy and precision better than   379
5 cm, which systems like GPS cannot deliver. Thus, the aforementioned stroke level   380
metrics from available systems should be recognized as approximations. These   381
instrumentation limitations prevent direct and more sensitive investigations of the   382
complex causal relationships that exist between rower-oar-boat system mechanics and   383
boat performance at and within the level of an individual stroke. For these purposes,   384
this study explored methods for building more accurate and precise measures of boat   385
movement. We built a system using consumer electronics and services and focused on   386
designing a general purpose and easy-to-use solution that could be broadly deployed in   387
the rowing community.   388
   We presented two alternative estimation methods for boat distance traveled, boat   389
speed, and distance per stroke. They both perform much better than the direct output   390
from the smartphone and have similar performance between the two but neither reaches   391
the 5 cm level of accuracy. The complementary filter has the disadvantage that the   392
filter cutoff frequencies aren't updated to optimal values in real-time, and the optimal   393
offline values we use do not robustly handle all stroke rates for the two rowers and boats   394
investigated. This makes the Kalman filter method more attractive because the bias   395
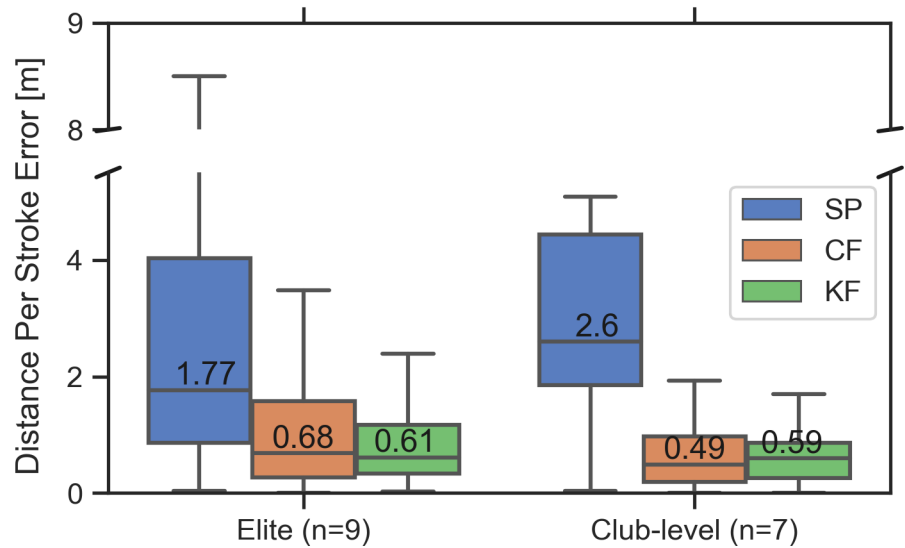
Fig 15. Summary of the distance per stroke error for all strokes.
Comparison of the distance per stroke error relative to the DGPS-derived value for all
trials for the elite and club-level rowers, respectively.

term is adaptively updated for every rower and boat. The filter tunes itself. Both filters
take time to converge to a steady error from a zero speed start, so the first strokes in a
race will produce less accurate results. A future study could look into minimizing the
startup time by tuning the filters further, but there is likely a tradeoff in accuracy and
precision of the estimations.

Both of our presented methods provide better estimates of boat speed and distance
traveled per stroke that any prior work that uses a single low-cost commercially
available GPS system. The closest prior work on rowing is the thesis from Hermsen [21].
Hermsen's concept was similar but did not offer the online adaptation that our Kalman
filter design provides and there were no reported improvements in any metric but
predicted time. Our methods do not provide estimates as accurate as differential GPS
systems, but for the cost and convenience trade-off our methods are likely more
attractive for many use cases.

We sought to develop a general purpose boat-moving model that was independent of
stroke rate, and the models presented in this paper were constructed from experiments
involving single rowers assigned rowing rates that ranged from 16 to 34 strokes per
minute. The markedly inferior performance of distance per stroke measures in the SP
model relative to the CF and KF models is largely attributed to the smartphone's
limitation of only a relatively low sampling frequency of location. In the case of high
stroke rate rowing where stroke frequency (at the high end faster than 0.5 Hz) exceeds
the smartphone location sampling frequency (0.3-0.5 Hz), there are numerous instances
between location samples where a stroke ends, a second stroke is completed, and a third
stroke begins. In these cases, the distance per stroke error of the second stroke is the
entire distance traveled. Accordingly, the CF and KF models stand to add the most
value for high rate rowing, *e.g.*, racing rates. It may be possible to further improve
model accuracy by relaxing the general purpose model constraint and building more
special purpose models, *e.g.*, model parameters tuned to ranges of rowing rates, rowing
ability, boat class, etc. Relatively expensive commercial sports position and speed

sensors can sample position at higher rates than a smartphone and thus can be a useful ₄₂₄ method of addressing the significantly large errors that the low frequency sampling of ₄₂₅ location of the smartphone model creates. However, these high frequency sampling ₄₂₆ solutions do not eliminate the inaccuracies and imprecision of the position ₄₂₇ measurements and thus do not represent a viable method for achieving the goal of ₄₂₈ distance per stroke accuracy of 5 cm or less. Once we realize model improvements that ₄₂₉ can achieve this level of accuracy and thus enable more microscopic analyses of rowing ₄₃₀ mechanics, we anticipate the emergence of a new generation of tools for testing and ₄₃₁ coaching the improvement of boat-moving performance. ₄₃₂

Conclusion ₄₃₃

We have presented two methods to estimate the distance, speed, and distance per stroke ₄₃₄ along a rowing boat's path in real time that provide high accuracy and precision from ₄₃₅ the relatively low accuracy sensors in a single smartphone attached to the boat. These ₄₃₆ estimates provide an intimate view of the rower's performance. In particular, we show ₄₃₇ that the distance per stroke can be estimated to an accuracy of 50 cm which is ₄₃₈ improved but not good enough to be able to examine relative stroke differences that ₄₃₉ may contribute to winning or losing a race. Additionally, the inter-stroke view of boat ₄₄₀ speed that our methods provide is better than any inexpensive commercial on-board ₄₄₁ boat speed measurement device and begins to compare favorably to very accurate ₄₄₂ differential GPS systems without the need for more than one GPS receiver. Overall, ₄₄₃ this paper demonstrates the power that carefully crafted, activity-specific sensor fusion ₄₄₄ algorithms can have even with poor accuracy sensors. MEMs based inertial ₄₄₅ measurement units, like those found in smartphones, are continually decreasing in cost ₄₄₆ and size and will play a larger role in collecting field data in sports. However, the utility ₄₄₇ of these systems will depend on the development and improvement of ₄₄₈ application-specific sensor fusion algorithms. ₄₄₉

Nomenclature ₄₅₀

Complementary Filter ₄₅₁

A Smartphone accelerometer input signal ₄₅₂

a_0 Acceleration bias ₄₅₃

D Smartphone GPS input signal ₄₅₄

H Transfer function ₄₅₅

s Denotes the frequency domain $(s = jw)$ ₄₅₆

w Frequency [Hz] ₄₅₇

w_c Cutoff frequency [Hz] ₄₅₈

X Input signal ₄₅₉

Y Output signal ₄₆₀

Error Calculations ₄₆₁

$\bar{d}_e, \bar{v}_e$ Mean error of distance estimate and the speed estimate, respectively, relative to ₄₆₂ the differential GPS derived value ₄₆₃

CE_{d_e,v_e} Central error of the distance and speed, resp. relative to the differential GPS derived value

RMSE_{d,v,d_s} Root mean square error of the distance, speed, and distance per stroke, resp., relative to the differential GPS derived value

$\mathrm{Var}(d_e,v_e)$ Variance of the distance error and speed error, resp., relative to the differential GPS derived value

d_e, v_e Error in distance estimate and the speed estimate, resp., relative to the differential GPS derived value

Kalman Filter

α_{yk} KF input: smartphone longitudinal acceleration component

$\boldsymbol{\nu}_k$ KF measurement noise vector

$\mathbf{A}$ KF state transition matrix

$\mathbf{B}$ KF input matrix

$\mathbf{C}$ KF output matrix

$\mathbf{D}$ KF feed-through matrix

$\mathbf{L}_k$ KF gain matrix

$\mathbf{P}_k$ KF estimate covariance

$\mathbf{Q}$ KF process noise covariance matrix

$\mathbf{R}$ KF measurement noise covariance matrix

$\mathbf{u}_k$ KF input vector

$\mathbf{w}_k$ KF process noise vector

$\mathbf{x}_k$ KF state vector

$\mathbf{y}_k$ KF output vector

ϕ_k KF state: accelerometer bias $[\mathrm{m\,s^{-2}}]$

a_k KF input: acceleration

d_k KF state: distance $[\mathrm{m}]$

v_k KF state: speed $[\mathrm{m\,s^{-1}}]$

Other Symbols

$\alpha_{x,y,z}$ Smartphone body-fixed acceleration components $[\mathrm{m\,s^{-2}}]$

$\boldsymbol{\alpha}$ Boat mounted body-fixed smartphone acceleration vector $[\mathrm{m\,s^{-2}}]$

Δt Time differential $[\mathrm{s}]$

a Magnitude of the acceleration along the boat's path $[\mathrm{m\,s^{-2}}]$

d Distance traveled along the boat's path $[\mathrm{m}]$

d_s Distance per stroke $[\mathrm{m\,s^{-1}}]$

d_s	Distance per stroke	498
t	Time	499
v	Magnitude of the velocity along the boat's path	500
x	East-West position on the local WGS84 plane [m]	501
y	North-South position on the local WDGS84 plane [m]	502
CF	Abbreviation for complementary filter	503
KF	Abbreviation for Kalman filter	504
SP	Abbreviation for smartphone	505

Acknowledgments 506

References 514

1. Winter DA. Biomechanics and Motor Control of Human Movement. John Wiley 515
   & Sons; 2009. 516

2. Lee L, Jones M, Ridenour GS, Bennett SJ, Majors AC, Melito BL, et al. 517
   Comparison of Accuracy and Precision of GPS-Enabled Mobile Devices. In: 2016 518
   IEEE International Conference on Computer and Information Technology (CIT); 519
   2016. p. 73–82. 520

3. Zhizhong Ma, Yuansong Qiao, Lee B, Fallon E. Experimental Evaluation of 521
   Mobile Phone Sensors. In: 24th IET Irish Signals and Systems Conference (ISSC 522
   2013). Letterkenny, Ireland: Institution of Engineering and Technology; 2013. p. 523
   49–49. 524

4. Smith TB, Hopkins WG. Measures of Rowing Performance. Sports Medicine. 525
   2012;42(4):343–358. doi:10.2165/11597230-000000000-00000. 526

5. Kleshnev V. Biomechanics of Rowing. Crowood Press; 2016. 527

6. Cejuela Anta R, Turpin P, Antonio J, Cortell-Tormo JM, Mira C, José J. An 528
   Analysis of High Performance in Long-Distance Rowing by Means of Global 529
   Positioning System Technology. In: Symposium Proceedings 6TM IACSS; 2008. 530
   p. 1–4. 531

7. Simões ND, Gonçalves JL, Caeiro ML, Boavida MJ, Cardoso FD. ZigBee/GPS 532
   Tracking System for Rowing Races. In: 2011 IEEE EUROCON - International 533
   Conference on Computer as a Tool; 2011. p. 1–4. 534

8. Ai K, He S. Development of a Speed Measurement System with Globle   535
   Positioning System in Rowing and Canoeing. ISBS - Conference Proceedings   536
   Archive. 2000;1(1).   537

9. Zhang K, Deakin R, Grenfell R, Li Y, Zhang J, Cameron WN, et al. GNSS for   538
   Sports ? Sailing and Rowing Perspectives. Journal of Global Positioning Systems. 539
   2004;3(1&2):280–289. doi:10.5081/jgps.3.1.280.   540

10. Hedgecock W, Maroti M, Sallai J, Volgyesi P, Ledeczi A. High-Accuracy   541
    Differential Tracking of Low-Cost GPS Receivers. In: MobiSys 2013. ACM Press; 542
    2013. p. 221.   543

11. Kiam JJ, Cardenas JM, Henkel P. Cost-Effective Cooperative RTK Positioning 544
    for Rowing Boats. In: Proc. of ION International Technical Meeting (ITM); 2014. 545
    p. 541–550.   546

12. Hill H, Fahrig S. The Impact of Fluctuations in Boat Velocity during the Rowing 547
    Cycle on Race Time. Scandinavian Journal of Medicine & Science in Sports.   548
    2009;19(4):585–594. doi:10.1111/j.1600-0838.2008.00819.x.   549

13. Waegli A, Skaloud J. Optimization of Two GPS/MEMS-IMU Integration   550
    Strategies with Application to Sports. GPS Solutions. 2009;13(4):315–326.   551
    doi:10.1007/s10291-009-0124-5.   552

14. Groh BH, Reinfelder SJ, Streicher MN, Taraben A, Eskofier BM. Movement   553
    Prediction in Rowing Using a Dynamic Time Warping Based Stroke Detection.   554
    In: 2014 IEEE Ninth International Conference on Intelligent Sensors, Sensor 555
    Networks and Information Processing (ISSNIP); 2014. p. 1–6.   556

15. Janssen I, Sachlikidis A. Validity and Reliability of Intra-Stroke Kayak Velocity 557
    and Acceleration Using a GPS-Based Accelerometer. Sports Biomechanics.   558
    2010;9(1):47–56. doi:10.1080/14763141003690229.   559

16. Mpimis A, Gikas V. Monitoring and Evaluation of Rowing Performance Using   560
    Mobile Mapping Data. Archiwum Fotogrametrii, Kartografii i Teledetekcji.   561
    2011;Vol. 22.   562

17. Ruffaldi E, Peppoloni L, Filippeschi A. Sensor Fusion for Complex Articulated 563
    Body Tracking Applied in Rowing. Proceedings of the Institution of Mechanical 564
    Engineers, Part P: Journal of Sports Engineering and Technology.   565
    2015;229(2):92–102. doi:10.1177/1754337115583199.   566

18. Anderson R, Harrison A, Lyons GM. Accelerometry-Based Feedback–Can It   567
    Improve Movement Consistency and Performance in Rowing? Sports   568
    Biomechanics. 2005;4(2):179–195. doi:10.1080/14763140508522862.   569

19. Tessendorf B, Gravenhorst F, Arnrich B, Tröster G. An IMU-Based Sensor   570
    Network to Continuously Monitor Rowing Technique on the Water. In: 2011   571
    Seventh International Conference on Intelligent Sensors, Sensor Networks and 572
    Information Processing; 2011. p. 253–258.   573

20. Schindhelm CK, Gschwandtner F, Banholzer M. Usability of Apple iPhones for 574
    Inertial Navigation Systems. In: 2011 IEEE 22nd International Symposium on   575
    Personal, Indoor and Mobile Radio Communications; 2011. p. 1254–1258.   576

21. Hermsen H. Using GPS and Accelerometer Data for Rowing Race Tracking   577
    [Master]. University of Groningen. Groningen, Netherlands; 2013.   578

22. NIMA. Department of Defense World Geodetic System 1984, Its Definition and Relationships With Local Geodetic Systems. National Imagery and Mapping Agency; 2000. TR8350.2.

23. Palshikar GK. Simple Algorithms for Peak Detection in Time-Series. In: 1st Int. Conf. Advanced Data Analysis, Business Analytics and Intelligence; 2009. p. 14.

24. van den Bogert AJ, Geijtenbeek T, Even-Zohar O, Steenbrink F, Hardin EC. A Real-Time System for Biomechanical Analysis of Human Movement and Muscle Function. Medical & Biological Engineering & Computing. 2013; p. 1–9. doi:10.1007/s11517-013-1076-z.

25. Kalman RE. A New Approach to Linear Filtering and Prediction Problems. Transactions of the ASME–Journal of Basic Engineering. 1960;82(Series D):35–45.

26. Grewal M, Andrews AP. Kalman FIltering: Theory and Practice Using MATLAB. 3rd ed. John Wiley & Sons, Inc; 2008.